Modeling Pointing Tasks in Human-Blimp Interactions

Mengxue Hou, Qiuyang Tao, Paul Varnell, Fumin Zhang

***Abstract*—We investigate interaction between human and a miniature autonomous blimp, by letting the human control position of the blimp through pointing motion. The blimp is controlled by a position feedback controller, with the reference position set to the position of pointer. We observe that the blimp can follow the pointing motion, and reach certain target position. Since the human intention represented by the desired target position for the blimp is not measurable during the process, the Vector Integration to Endpoint (VITE) model is applied to model the dynamics of human pointing motion and to identify the hidden human intention. Stability analysis shows that the closed-loop human-blimp dynamics are exponentially stable. Experimental data verifies that the VITE model is applicable to model human blimp interaction in 3D space, and the human intention can be identified from trajectories of the blimp and pointer movements.**

I. Introduction

The Georgia Tech Miniature Autonomous Blimp (GT-MAB) is a lighter-than-air Unmanned Aerial Vehicle (UAV) developed for indoor applications in human-occupied environment. It consists of a saucer-shaped envelop filled with Helium, and a gondola attached below the envelop. The envelop makes GT-MAB naturally cushioned, not posing any threat to human safety. Besides, due to the lifting power provided by the buoyancy of its envelop, GT-MAB keeps itself aloft without the need for consistent propulsion. Therefore, it is energy-efficient, and its endurance can be several magnitude longer than that of a heavier-than-air UAV [1]. The extended flight endurance makes it well-suited for many applications that require sustained airborne presence. Previous works on GT-MAB have been focused on its dynamics modeling and motion control [2]–[4], and vision-based Human Robot Interaction (HRI) [5], [6].

This work investigates interactions between a human subject and the GT-MAB to explore the potential of using pointing motion to control flight of the GT-MAB. Human pointing motion can serve as a more simple and intuitive user interface, which is desired [7]. Previous approaches to gesture-based robot control involve the use of predefined codebooks or dictionaries of gestures. Mapping methods are developed to translate from human gestures to robot behaviors. Existing research on designing intuitive gestures are mostly focused on controlling quad-rotors in both indoor and outdoor experiments [8]–[10]. However, due to the high flying speed of quad-rotors, for safety concerns, these gestures are not tested for HRI experiments in confined space where human and the vehicle are in close proximity. Our approach allows human to control the flying blimp with pointing motion that is commonly used in graphical user interface design (e.g. moving a computer mouse to click on a button), while the human and the blimp are close to each other. This allows us to identify the characteristics of human pointing motion that is different from using a computer mouse or commanding a quad-rotor.

During the interaction experiments, the human uses a marked wand as the pointer, which is traced by a localization system. The wand position was transmitted to the blimp. Then we implement a feedback controller for the GT-MAB so that it can follow the pointing motion of human during the experiments. The human perceives the blimp position, and moves the wand to guide the blimp towards a target position. The human stops moving the wand when he/she is satisfied with the blimp's current position. The intention of the human, which is the goal position that the human specifies, is not known by the blimp.

We propose an algorithm to identify human's intention, given trajectories of the wand and the blimp. This is challenging since there is no existing model describing the dynamics of human's pointing motion when interacting with a flying object in 3D space. We found the VITE model [11], which describes the endpoint movement of human reaching and pointing motion in other settings e.g. computer interface [12]–[15], can be applied to model human-blimp interaction. The human specified target position is identified by fitting the VITE model with the collected data using the Nonlinear Least Squares (NLS) method. Theoretical analysis shows stability of the closed-loop feedback system where VITE model is integrated with blimp dynamics. To the best of our knowledge, this is the first HRI demonstration where human pointing motion is studied in the context of human interacting with a flying vehicle.

The rest of the paper is organized as follows. The problem formulation, introduction on background of this paper, as well as analysis of stability are presented in Section II. Experiment setting and experiment results are shown in Section III. Section IV describes the conclusion of the paper based on the experiment results.

Mengxue Hou, Qiuyang Tao, Paul Varnell and Fumin Zhang are with the School of Electrical and Computer Engineering, Georgia Institute of Technology, Atlanta, Georgia 30308, {mhou30, qtao7, jvarnell3, fumin}@gatech.edu

II. Problem Formulation

In this section, we will first present the mathematical formulation of the problem, then briefly describe the VITE model, the dynamics of GT-MAB, and provide stability analysis of the close-loop system describing the human-blimp interaction through pointing motion.

Consider that the blimp is controlled by a feedback waypoint controller, with the reference waypoint set to the position of the wand that the human is holding. We use $\mathbf{y}(t) \in \mathbb{R}^3$ to denote the position of the wand at time t, and $\mathbf{u}(t) \in \mathbb{R}^3$ to describe position of GT-MAB. The human is asked to determine a target position in the 3D space which is unknown to the blimp, represented as $\mathbf{r}_t \in \mathbb{R}^3$. Then the human is asked to drive the blimp from its initial position towards the target position by moving the wand. One trial of experiment is considered to be finished when the human is satisfied with the blimp position, whether or not it reaches the target position. The interaction dynamics can be illustrated by block diagram shown in Figure 1. The human operator observes $\mathbf{u}(t)$, then moves the wand position, $\mathbf{y}(t)$ according to certain dynamics. The blimp obtains the updated wand position, and follows the wand position according to the feedback law. We assume that there is no delay or perturbation in human observing the blimp motion, or in the blimp reacting to movement of the wand.

Let us describe the wand position dynamics as

$$\dot{\mathbf{y}}(t) = f(\mathbf{u}(t), \mathbf{r}_t), \tag{1}$$

where f is an unknown function mapping blimp position and target position to the wand motion. In this work, the goal is to identify the unknown function f, and also identify the target position that human implicitly specifies, given the wand and blimp trajectories.

In order to simplify the problem, we have the following assumptions.

Assumption 1. *We assume that the target position that the human specifies has the same horizontal position as blimp's initial position. Then the blimp and the wand only have vertical movement, but no horizontal movement throughout the experiment.*

Remark 1. *This assumption allows us to simplify the wand and blimp dynamics to movement in only one direction. In fact, with proper coordinate transformation, it is easy to drop this constraint, and apply the current analysis to linear motion in the 3D space.*

Due to Assumption 1, we will simplify $\mathbf{u}(t)$, $\mathbf{y}(t)$ and $\mathbf{r}_t$ into scalars representing only the height of the blimp, the wand and the target position.

A. VITE Model

It has been shown that human exhibits similar motions when reaching and pointing with their arms, mouse pointers and other devices [16]. The dynamics of human reaching and pointing motion can be described by the VITE model, which is a widely accepted dynamic model describing motion governed by an agonist-antagonist pair of muscles. It is given by

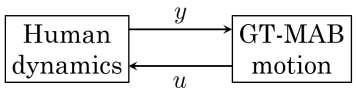

Fig. 1. Block diagram of the closed loop pointing motion model.

$$\begin{cases} \dot{\eta}(t) = \gamma(-\eta(t) + r_t - u(t)) \\ \dot{y}(t) = g[\eta(t)]_d^+ \end{cases}, \tag{2}$$

where $u(t)$ represents the perceived position of the pointer, r_t denotes the perceived desired position of the pointer, $r_t - u(t)$ is noted as a difference vector describing the difference between the pointer position and the desired position. $\eta(t)$ represents an internal state describing how the human perceives the difference between target position and pointer position, which cumulatively integrates all the difference vectors through time, with a constant gain γ. The operator $[\cdot]_d^+$ is used to switch the pointing motion off when the pointer overshoots its target. It is defined by the following equation

$$[v]_d^+ = \begin{cases} v, & \text{if } \langle v, d \rangle \geq 0 \\ 0, & \text{otherwise} \end{cases}, \tag{3}$$

where d defines the direction from the pointer to the target position at initial time. g is called the go signal, and is a feedback gain describing how the internal state $\eta(t)$ results in pointer motion. The true pointer position that is controlled by the user is represented by $y(t)$. The VITE model is widely used in human computer interface to describe the motion of a person trying to drive the cursor position $u(t)$ to the target position r_t, by controlling the position of the mouse $y(t)$. In the human and GT-MAB interaction case, position of GT-MAB that human perceives will be the perceived cursor position in the human computer interface case, while the wand controlled by the human will be the mouse.

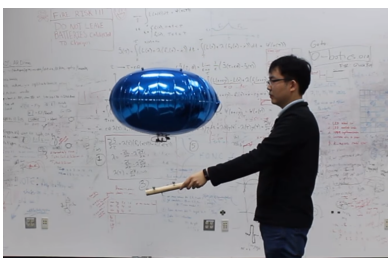

Fig. 2. Picture of a human interacting with GT-MAB through pointing with the wand.

B. GT-MAB Flight Controller

From our previous work [2], [4], the vertical motion of GT-MAB can be described as

$$m\dot{w}(t) = F_z(t) + f_z(t), \tag{4}$$

where m is the total mass of the robot, ω is the vertical speed, $F_z(t)$ and $f_z(t)$ represents the aerodynamic drag and the thrust force projected onto the vertical direction.

Feedback controllers are implemented to control the position and heading of the blimp. For convenience, GT-MAB keeps the same heading angle through the entire experiment, and the reference setpoint for horizonal movement is set to a fixed position, so that it will remain at the same horizontal position throughout the experiment. Setpoint of the vertical motion is set to height of the wand, thus enabling the blimp to track position of the wand. The height controller can be described as

$$f_z(t) = k_p e(t), \tag{5}$$

where $e(t) = u(t) - y(t)$ represents the difference between height of the blimp and the height of the wand. $k_p < 0$ denotes the feedback gain.

C. Stability Analysis

Given the blimp dynamics described in Eq. (5), and the human pointing motion dynamics as given by the VITE model given in Eq. (2), we can connect the two models, as shown in Figure 1 to create a closed loop pointing model. We make a few assumptions to simplify the following analysis. First, we assume that the aerodynamic drag term in Eq. (4) is proportional to blimp speed $w(t)$,

$$F_z(t) = -Hw(t), \tag{6}$$

where $H > 0$ denotes a constant gain. We make the second assumption that the target position is located at the origin 0. In general, this can be achieved by coordinate frame transformation. Also, for the stability analysis in this section, we will focus on only one going-up section, that is, the initial position of the blimp is lower than the target position, meaning $u(0) < 0$, and the direction from the pointer to the target position, defined in Eq. (2), is $d > 0$. We also assume that at the starting time $t = 0$, human perceives a difference between the blimp position and the target position, indicating that $\eta(0) > 0$. Given these assumptions, we define an augmented state $\mathbf{x} \in \mathbb{R}^4$, and elements of $\mathbf{x}$ are defined as $\begin{bmatrix} x_1 & x_2 & x_3 & x_4 \end{bmatrix}^T := \begin{bmatrix} u & \eta & \dot{u} & y \end{bmatrix}^T$, then the closed loop system dynamics can be written as

$$\dot{\mathbf{x}} = \begin{bmatrix} x_3 \\ -\gamma(x_1 + x_2) \\ -Hx_3 + k_p(x_1 - x_4) \\ g x_2^+ \end{bmatrix}, \tag{7}$$

where x_2^+ denotes the positive part of x_2, that is, $p^+ = p$ when $p \geq 0$, and $p = 0$ when $p < 0$.

We will now examine the stability of the closed loop system dynamics in Eq. (7) considering two cases, the first case where $x_2 \geq 0$, and the second case $x_2 < 0$. In both two cases, the system dynamics is linear, while a switch in system dynamics happens when x_2 goes from $x_2 > 0$ to $x_2 < 0$. Define a vector $\mathbf{z} \in \mathbb{R}^4$ as

$$\mathbf{z} = \begin{bmatrix} x_1 - x_4 & x_1 + x_2 & x_3 & x_2^+ \end{bmatrix}^T.$$

In the case where $x_2 \geq 0$,

$$\dot{\mathbf{z}} = \begin{bmatrix} 0 & 0 & 1 & -g \\ 0 & -\gamma & 1 & 0 \\ k_p & 0 & -H & 0 \\ 0 & -\gamma & 0 & 0 \end{bmatrix} \mathbf{z} := \mathbf{A}_1 \mathbf{z}.$$

In the case where $x_2 < 0$, $z_4 = x_2^+ = 0$. Thus, $\dot{z}_4 = 0$, and the dynamics of $\mathbf{z}$ can be described as

$$\dot{\mathbf{z}} = \begin{bmatrix} 0 & 0 & 1 & 0 \\ 0 & -\gamma & 1 & 0 \\ k_p & 0 & -H & 0 \\ 0 & 0 & 0 & 0 \end{bmatrix} \mathbf{z} := \mathbf{A}_2 \mathbf{z}.$$

Lemma 1. *The closed-loop system $\dot{\mathbf{z}} = \mathbf{A}_1 \mathbf{z}$ is exponentially stable if $H, g, \gamma > 0, k_p < \gamma^2(1 - \frac{g}{H}) + \gamma(H - 2g) - gH$.*

Proof. We will prove the above lemma using Routh's stability criterion. The characteristic polynomial is

$$\begin{aligned} \det(\lambda I - A_1) = \lambda^4 + (H + \gamma)\lambda^3 \\ + (\gamma H - k_p)\lambda^2 - \gamma k_p \lambda - g k_p \gamma. \end{aligned} \tag{8}$$

The matrix A_1 is Hurwitz if the first column of the Routh array is positive. Denote the first column of the Routh array as a_1, a_2, b_1, c_1, d_1. a_1, a_2, b_1 and d_1 are guaranteed to be positive given any choice of $H, \gamma, g > 0, k_p < 0$. If $c_1 > 0$, then $k_p < \gamma^2(1 - \frac{g}{H}) + \gamma(H - 2g) - gH$. □

Then we will consider the case where $x_2 < 0$. Since in this case, z_4 has already converges to the equilibrium point, we will consider the stability of the subsystem $\dot{\tilde{\mathbf{z}}} = \tilde{\mathbf{A}}_2 \tilde{\mathbf{z}}$, where $\tilde{\mathbf{z}} = [z_1, z_2, z_3]^T$, $\tilde{\mathbf{A}}_2$ is the third order leading principal submatrix of $\mathbf{A}_2$.

Lemma 2. *The subsystem $\dot{\tilde{\mathbf{z}}} = \tilde{\mathbf{A}}_2 \tilde{\mathbf{z}}$ is exponentially stable for all $H, g, \gamma > 0, k_p < 0$.*

Proof. The characteristic polynomial is

$$\det(\lambda I - A_2) = \lambda^3 + (H + \gamma)\lambda^2 + (\gamma H - k_p)\lambda - k_p \gamma.$$

For all $H, g, \gamma > 0, k_p < 0$, the first column of the Routh array is positive. Therefore, the closed-loop system is exponentially stable. □

Given the discussion above, the above two Lemmas lead to the following Theorem.

Theorem 1. *For the system dynamics described by Eq. (7), with* $H, g, \gamma > 0, k_p < \gamma^2(1-\frac{g}{H})+\gamma(H-2g)-gH$, *if the states* $\mathbf{x}$ *start from the region* $x_2 > 0$, *the states will exponentially converge to the equilibrium set*

$$E = \{x_3 = 0, \text{ and } x_1 = x_4 = -x_2, \text{ and } x_2 \leq 0\}. \quad (9)$$

Proof. If the states start from the region $x_2 > 0$, due to the exponential stability of $\dot{\mathbf{z}} = \mathbf{A}_1\mathbf{z}$, there will be either zero switch or one switch along the trajectory. In the case of no switch, the states will exponentially converge to the equilibrium set. In the case of one switch, let t_1 denote the time when the system dynamics switches. From Lemma 1, $\exists\ m_1, \alpha_1, \epsilon_1 > 0$, such that $||\mathbf{z}(t)|| \leq m_1 e^{-\alpha_1 t}||\mathbf{z}(0)||$, for all $||\mathbf{z}(0)|| \leq \epsilon_1, t \in [0, t_1)$. From Lemma 2, $\exists\ m_2, \alpha_2, \epsilon_2 > 0$, such that $||\tilde{\mathbf{z}}(t)|| \leq m_2 e^{-\alpha_2(t-t_1)}||\tilde{\mathbf{z}}(t_1)||$, for all $||\tilde{\mathbf{z}}(t_1)|| \leq \epsilon_2, t \in [t_1, \infty)$. Since $z_4 = 0$, $||\mathbf{z}(t)|| = ||\tilde{\mathbf{z}}(t)||$. Therefore,

$$||\mathbf{z}(t)|| \leq \max(m_1 m_2, m_1) e^{-\min(\alpha_1, \alpha_2)t}||\mathbf{z}(0)||,$$

for all $||\mathbf{z}(0)|| \leq \epsilon_1$, $t \in [0, \infty)$. Thus the switching system is exponentially stable, and will converge to the equilibrium $\mathbf{z} = 0$. The states $\mathbf{x}$ will exponentially converge to the equilibrium set $E = \{x_3 = 0, \text{ and } x_1 = x_4 = -x_2, \text{ and } x_2 \leq 0\}$. □

III. Experiment Result

In this section, we will describe the experiment setting, and present the experimental data. The experimental data is processed in order to identify the unknown parameters of the system. Accuracy of modeling and parameter identification is discussed. Besides, stability of the closed-loop system is also verified given parameters identified from experimental data.

A. Experiment Setting

In one of the experiments, the participant is a developer of GT-MAB and is familiar with its dynamics. We asked the participant to choose two target positions of different heights, and drive the blimp from starting position to the first target position by moving the wand. Once the participant is satisfied with the blimp position, he will drive the blimp towards the second target position. The participant is asked to keep repeating this task during 100 seconds.

The experiment took place in a space that is 8 m long, 7.5 m wide, and 3.5 m high. Flex13 cameras from OptiTrack are installed on the walls, at about 3.5 m height. Reflective markers are attached on the top of GT-MAB envelop as well as on the tip of the wand, so that the OptiTrack system can detect and record position of the wand and the blimp. Considering the limited coverage of OptiTrack cameras, the human and the blimp will stay inside a 4 m long, 4 m wide, and 2 m high space during the experiment. The starting position of blimp is about 1 m away from the human, and is about 1.5 m high, while the horizontal target position of the blimp will be the same as the starting position, and the vertical target position will be between 0.5 m and 2 m. Figure 3 shows a demonstration of the experiment settings.

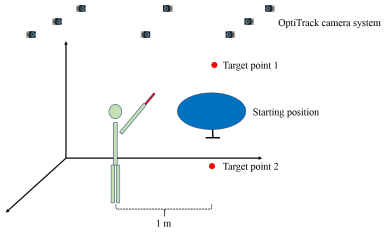

Fig. 3. Demonstration of experiment settings. OpiTrack camera system is installed on the walls to measure GT-MAB and wand trajectories. The horizontal position of human is about 1 m away from the horizontal position of GT-MAB.

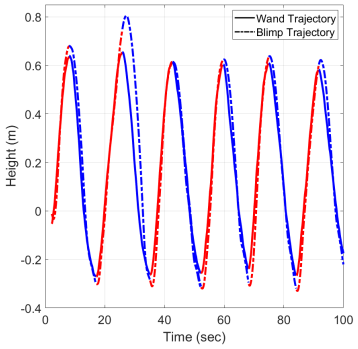

Fig. 4. Blimp trajectory and wand trajectories divided into going-up and going-down sections. Red represents the going-up sections while blue represents the going-down sections.

B. Parameter Estimation

Since the human is driving the blimp to two different target positions, we divide the wand and the blimp trajectories into two sections, the going-up section and the going-down section. Since the trial is considered to be finished once the human stops moving the wand, indicating that the human is satisfied with the blimp height, the time interval of the experiment can be divided into $[0, T_1], [T_1, T_2], \ldots, [T_{N-1}, T_N]$ based on the up/down motion of the wand. Let $\Omega_{up} = \{n \in \mathbb{Z} | \dot{y}(t) > 0, t \in [T_{n-1}, T_n]\}$ represent the set of all going-up sections. Similarly, let $\Omega_{down} = \{n \in \mathbb{Z} | \dot{y}(t) < 0, t \in [T_{n-1}, T_n]\}$ denote the set of going-down sections.

Let $r_{t,u}$ and $r_{t,d}$ represent the target position of all the going-up sections and going-down sections respectively. Then we find the set of parameters that fits the experimental data by minimizing the integrated difference between the true wand trajectory from experimental data and the simulated wand trajectory over all going-up

and going-down sections. Since the initial value of the internal state of each section is unknown, the initial values are also added to the parameters as a quantity with respect to which the fit is optimized. Denote the set of initial values of $\eta(t)$ in each of the sections as $\Xi = \{\eta(t)|t \in \{0, T_1, \ldots, T_{N-1}\}\}$, then the set of parameters that will be estimated can be represented as $\Pi = [\hat{r}_{t,u}, \hat{r}_{t,d}, \hat{\gamma}, g, \hat{\Xi}]$. The NLS problem can be formulated as

$$\begin{aligned}
&\min_{\Pi} \sum_{n\in\Omega_{up}} \int_{T_{n-1}}^{T_n} (y(t)-\hat{y}(t))^2 dt \\
&+ \sum_{n\in\Omega_{down}} \int_{T_{n-1}}^{T_n} (y(t)-\hat{y}(t))^2 dt \\
&\text{s.t. } \dot{\hat{\eta}}(t) = \begin{cases} \gamma(-\hat{\eta}(t) + r_{t,u} - u(t)), \text{ if } n \in \Omega_{up} \\ \gamma(-\hat{\eta}(t) + r_{t,d} - u(t)), \text{ if } n \in \Omega_{down} \end{cases}, \\
&\quad \dot{\hat{y}}(t) = g[\hat{\eta}(t)]_d^+, \\
&\quad \hat{y}(0) = y(0), \\
&\quad \hat{\Xi}_n > 0, \text{ if } n \in \Omega_{up};\ \hat{\Xi}_n < 0, \text{ if } n \in \Omega_{down},
\end{aligned} \tag{10}$$

where $y(t)$ represents the true wand trajectory from the experimental data, $\hat{y}(t)$ describes the simulated wand trajectory. The simulated wand trajectory is initialized with the same initial value as the true trajectory. Since at the beginning of each section, human perceives a difference between the target position and the blimp position, we pose a constraint on the initial condition of $\hat{\eta}(t)$ in each section, that the n^{th} element of $\hat{\Xi}$, denoted as $\hat{\Xi}_n$ is positive if $n \in \Omega_{up}$, and is negative if $n \in \Omega_{down}$.

C. Results and Discussion

With the collected data, we first divide the trajectory into going-up and going-down sections. Figure 4 shows blimp and wand trajectories divided into up/down sections. Identified parameters, including the target position, the estimated feedback gain and the go signal, are shown in Figure 5. The identified target position for up/down sections are 0.9348 m and -0.4206 m, respectively. The identified feedback gain and the go signal value are $\gamma = 0.268$, $g = 0.1448$.

The performance of parameter identification can be verified by comparing the wand trajectory measured in experiment with the wand trajectory simulated from the VITE model with the identified parameters. From Figure 6, the simulated trajectory matches with the true trajectory from experiment. The Root Mean Square Error (RMSE) between the true and the simulated wand trajectory is 0.0463 m, which is approximately 5.7% of the total change-of-height throughout the experiment. Therefore, the simulated wand trajectory is an accurate fit of the true wand trajectory, indicating that the VITE model is applicable to modeling human pointing motion when interacting with the blimp.

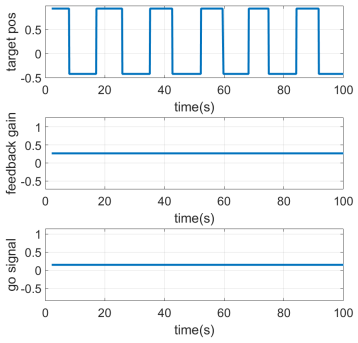

Fig. 5. Identified target position implicitly determined by the human, and the identified feedback gain and go signal value in the VITE model.

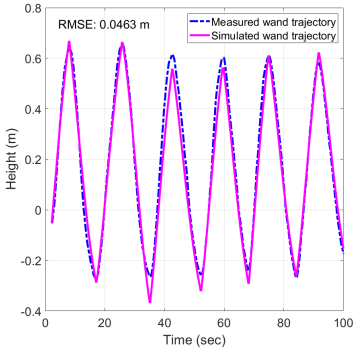

Fig. 6. Comparison between the wand trajectory from experimental data with the simulated wand trajectory from VITE model.

Further, given the parameters identified from experimental data, stability of the system can be shown given the stability condition presented in Theorem 1. The identified feedback gain and the go signal are given in Figure 5. Accurate estimation of H is difficult to derive, since it is related to the physical condition of each individual blimp during each experiment. Minor differences between experiments, such as the difference in volume of Helium in the envelop, difference in gondola placement position, etc., might have influence on the value. We linearize the dynamic model of blimp described in [2], and derive an estimation of $H \in (2, 4)$. During the experiment, the feedback gain of the controller is chosen to be $k_p = -1.312$, which satisfies the stability condition described in Theorem 1 for all possible values of H. Therefore, the closed-loop system with the identified parameters is exponentially stable.

It is observed from the experimental data that there is difference between human behavior when interacting with the computer mouse and the blimp through pointing motion. Figure 7 shows trajectories of the closed-loop

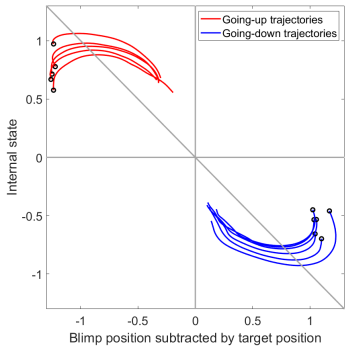

Fig. 7. Trajectories of the closed-loop pointing system. The x-axis represents the measured blimp position from experiment, with coordinate frame transformed to let the target position locate at the origin. The y-axis represents the simulated human internal state $\eta(t)$. The black circles indicate the initial position of trajectory in each of the up/down sections.

pointing system. Since the up/down sections are truncated when the wand stops moving, the ending point of each trajectory represents the system state when the human is satisfied with the blimp position. Figure 7 indicates that for both the going-up and going-down sections, the human is satisfied with the blimp position, and stops moving the wand prior to the time when $\eta = 0$, which is the time when the human perceives no difference between the blimp and the target position. This is different from the human behavior when interacting with a computer mouse, in which case the human stops moving the wand at the time when there is no perceived difference between the mouse and the target position [14]. One possible reason for human exhibiting behavior different from interacting with a computer mouse when interacting with the blimp is the limited thrust of GT-MAB. Due the limited thrust, the blimp may not be able to keep up with the wand movement. The insensitivity of blimp reacting to the wand movement may result in the human satisfied with blimp position even when there is still noticeable difference between the blimp and the target position.

IV. Conclusion

We investigate interaction between human and an autonomous blimp by letting the human control position of the blimp through pointing motion, to drive the blimp towards a target position specified by the human. The blimp is controlled by a position feedback controller, with the reference position set to the position of the pointer. We apply the VITE model to model the human motion when interacting with the blimp, and also to identify the unknown human intention, which is the target position. Stability analysis shows that the closed-loop system describing the human-blimp interaction through pointing motion is exponentially stable. Experimental data verifies that the VITE model is applicable to modeling human behavior in interacting with GT-MAB, and the human intention can be identified by fitting the VITE model to the experimental data.

References

[1] Y. B. Sebbane, *Lighter than Air Robots*. Springer Netherlands, 2012.

[2] S. Cho, V. Mishra, Q. Tao, P. Varnell, M. King-Smith, A. Muni, W. Smallwood, and F. Zhang, "Autopilot design for a class of miniature autonomous blimps," in *IEEE Conference on Control Technology and Applications, Kohala Coast, Hawaii*, 2017.

[3] Q. Tao, M. King-Smith, A. Muni, V. Mishra, S. Cho, P. Varnell, and F. Zhang, "Control theory - autonomous blimp," in *IEEE CSS Video Clip Contest*, 2015.

[4] Q. Tao, J. Cha, M. Hou, and F. Zhang, "Parameter identification of blimp dynamics through swinging motion," in *2018 15th International Conference on Control, Automation, Robotics and Vision*, 2018, pp. 1186 – 1191.

[5] N. Yao, E. Anaya, Q. Tao, S. Cho, H. Zheng, and F. Zhang, "Monocular vision-based human following on miniature robotic blimp," in *Proceedings of 2017 American Control Conference*, Seattle, WA, 2017.

[6] N. Yao, Q. Tao, W. Liu, Z. Liu, Y. Tian, P. Wang, T. Li, and F. Zhang, "Autonomous flying blimp interaction with human in an indoor space," *Frontiers of Information Technology and Electronic Engineering*, vol. 20, no. 1, pp. 45–59, 2019.

[7] M. A. Goodrich and A. C. Schultz, "Human-Robot Interaction: A survey," *Foundations and Trends in Human-Computer Interaction*, vol. 1, no. 3, pp. 203–275, Jan. 2007. [Online]. Available: http://dx.doi.org/10.1561/1100000005

[8] E. Peshkova, M. Hitz, and B. Kaufmann, "Natural interaction techniques for an Unmanned Aerial Vehicle system," *IEEE Pervasive Computing*, vol. 16, 2017.

[9] W. S. Ng and E. Sharlin, "Collocated interaction with flying robots," in *IEEE International Symposium on Robot and Human Interactive Communication*, 2011, pp. 143–149.

[10] K. Pfeil, S. L. Koh, and J. LaViola, "Exploring 3D gesture metaphors for interaction with Unmanned Aerial Vehicles," in *Proceedings of International Conference on Intelligent user interfaces*, 2013, pp. 257–266.

[11] D. Bullock and S. Grossberg, "Neural dynamics of planned arm movements: emergent invariants and speed-accuracy properties during trajectory formation," *Psychological Review*, vol. 95, no. 1, 1988.

[12] S. Aranovskiy, R. Ushirobira, D. Efimov, and G. Casiez, "Modeling pointing tasks in mouse-based Human-Computer Interactions," in *IEEE 55th Conference on Decision and Control*, 2016, pp. 6595 – 6600.

[13] P. Varnell and F. Zhang, "Characteristics of human pointing motions with acceleration," in *Proceedings of IEEE 54th Annual Conference on Decision and Control*, Osaka, Japan, 2015, pp. 5364–5369.

[14] P. Varnell, M. Malisoff, and F. Zhang, "Stability and robustness analysis for human pointing motions with acceleration under feedback delays," *International Journal of Robust and Nonlinear Control*, vol. 27, no. 5, pp. 703–721, 2016.

[15] P. Varnell and F. Zhang, "Dissipativity-based teleoperation with time-varying communication delays," in *Proceedings of 4th IFAC Workshop on Distributed Estimation and Control in Networked Systems*, Koblenz, Germany, 2013, pp. 369–376.

[16] R. Shadmehr and S. P. Wise, *The Computational Neurobiology of Reaching and Pointing*. MIT Press, 2005.